Impact of Assimilating AMSU-A Radiances on Forecasts of 2008 Atlantic Tropical Cyclones Initialized with a Limited-Area Ensemble Kalman Filter

ZHIQUAN LIU, CRAIG S. SCHWARTZ, CHRIS SNYDER, AND SO-YOUNG HA

National Center for Atmospheric Research, Boulder, Colorado*

(Manuscript received 15 March 2012, in final form 4 May 2012)

ABSTRACT

The impact of assimilating radiance observations from the Advanced Microwave Sounding Unit-A (AMSU-A) on forecasts of several tropical cyclones (TCs) was studied using the Weather Research and Forecasting Model (WRF) and a limited-area ensemble Kalman filter (EnKF). Analysis/forecast cycling experiments with and without AMSU-A radiance assimilation were performed over the Atlantic Ocean for the period 11 August–13 September 2008, when five named storms formed. For convenience, the radiance forward operators and bias-correction coefficients, along with the majority of quality-control decisions, were computed by a separate, preexisting variational assimilation system. The bias-correction coefficients were obtained from 3-month offline statistics and fixed during the EnKF analysis cycles. The vertical location of each radiance observation, which is required for covariance localization in the EnKF, was taken to be the level at which the AMSU-A channels' weighting functions peaked.

Deterministic 72-h WRF forecasts initialized from the ensemble-mean analyses were evaluated with a focus on TC prediction. Assimilating AMSU-A radiances produced better depictions of the environmental fields when compared to reanalyses and dropwindsonde observations. Radiance assimilation also resulted in substantial improvement of TC track and intensity forecasts with track-error reduction up to 16% for forecasts beyond 36 h. Additionally, assimilating both radiances and satellite winds gave markedly more benefit for TC track forecasts than solely assimilating radiances.

1. Introduction

Tropical cyclone (TC) track forecasts have steadily improved in the past two decades, but TC intensity forecast error has changed little over the same period (Rappaport et al. 2009). Substantial track error reduction can be attributed to general improvements in numerical weather prediction (NWP) modeling (dynamics, physical parameterizations, and higher spatial resolution), advancements in initialization and data assimilation (DA) techniques, and the assimilation of more observations, particularly those from satellite platforms. Since TCs are intense, isolated features, errors in short-range TC forecasts typically vary substantially in space and depend strongly on the location of the TC. Moreover, the fastest-growing errors are often associated with large gradients in the wind and mass fields (Puri et al. 2001). Therefore, accurate analyses of TC vortex structures and environments can be difficult and suboptimal with DA techniques using "climatological" background error covariances (BEC; e.g., Parrish and Derber 1992). However, ensemble-based DA techniques, such as the ensemble Kalman filter (EnKF; Evensen 1994; Burgers et al. 1998; Houtekamer and Mitchell 1998), may lead to better forecasts of TC intensity and a continued reduction of track error because of the use of flow-dependent error statistics estimated from short-term ensemble forecasts, which should represent spatial correlations and mass–wind balances better than static BECs in both the TC core and environment.

Several studies have focused on EnKF analyses of TC state with individual short-period case studies (e.g., Torn and Hakim 2009; Zhang et al. 2009, 2010; Li and Liu 2009; Liu and Li 2010) and extensive studies of multiple TCs in quasi-operational environments (e.g., Torn 2010;

* The National Center for Atmospheric Research is sponsored by the National Science Foundation.

Corresponding author address: Dr. Zhiquan Liu, National Center for Atmospheric Research, P.O. Box 3000, Boulder, CO 80307.
E-mail: liuz@ucar.edu

DOI: 10.1175/MWR-D-12-00083.1

Hamill et al. 2011a,b). They all showed that NWP model forecasts initialized with EnKF systems are competitive with or better than operational TC track and intensity forecasts. Among these studies, Li and Liu (2009) and Liu and Li (2010) demonstrated the positive impact of assimilating satellite retrievals of high-resolution (~15 km) temperature and moisture profiles from the Atmospheric Infrared Sounder (AIRS) on TC track and intensity forecasts.

Satellite radiance data are currently assimilated in many operational NWP centers with mostly variational DA algorithms and are one of the most important observation types for global NWP performance, especially over areas with sparse conventional observations (e.g., Derber and Wu 1998; McNally et al. 2000; Zapotocny et al. 2008). Several studies have directly assimilated radiances using an EnKF for global NWP models, but without the examination of radiance impact (Houtekamer et al. 2005; Buehner et al. 2010b; Miyoshi et al. 2010; Hamill et al. 2011a,b). Radiance assimilation efforts within the EnKF have been primarily devoted to better treatment of vertical error covariance localization (Houtekamer et al. 2005; Fertig et al. 2007; Miyoshi and Sato 2007; Campbell et al. 2010; Buehner et al. 2010a; Aravéquia et al. 2011) and bias correction (Fertig et al. 2009; Miyoshi et al. 2010; Aravéquia et al. 2011).

Although some studies have assimilated synthetic infrared radiances in cloudy conditions using ensemble-based methods with a limited-area model (e.g., Zupanski et al. 2011; Otkin 2010, 2012), real radiance data have rarely been assimilated with limited-area EnKF systems because polar-orbiting satellite coverage is nonuniform in a limited-area domain and bias correction is more challenging than in a global model. The recent study by Schwartz et al. (2012, hereafter SLCH) was the first attempt to assimilate microwave radiances with a limited-area EnKF and used the Weather Research and Forecasting Model (WRF; Skamarock et al. 2008) and the Data Assimilation Research Testbed (DART; Anderson et al. 2009), a system that we will hereafter term WRF/DART. Their results showed that assimilating microwave radiances with a limited-area EnKF produced overall improved forecasts of Typhoon Morakot (2009), although the precise effect differed among track, intensity, and rainfall forecasts. Following SLCH, this work further enhances radiance DA capability developed within WRF/DART and provides a robust second look at assimilating microwave radiances with a limited-area EnKF. Instead of a one-week case study as in SLCH, the impact of assimilating Advanced Microwave Sounding Unit-A (AMSU-A; Smith et al. 1979; Goodrum et al. 1999) radiances was evaluated for five Atlantic TCs for a month-long period during the summer of 2008.

A brief introduction to the EnKF algorithm is provided in section 2, followed by details of the radiance assimilation methodology in section 3. Section 4 gives an overview of the TC cases and section 5 describes the WRF configurations and experimental setting. Results are presented in section 6 before concluding in section 7.

2. Ensemble Kalman filter algorithm

Several variants of EnKF analysis algorithms exist. These fall into two categories: stochastic (Houtekamer and Mitchell 1998) and deterministic, based on whether perturbed observations are used to obtain the ensemble analysis. Deterministic filters can be further categorized as ensemble adjustment Kalman filter (EAKF; Anderson 2001), ensemble transform Kalman filter (Bishop et al. 2001), ensemble square root filter (Whitaker and Hamill 2002), and local ensemble transform Kalman filter (LETKF; Hunt et al. 2007). As noted by Tippett et al. (2003), the first three of these deterministic filters yield analysis ensembles with identical means and covariances when beginning from the same forecast ensemble (at least in the absence of covariance localization, discussed at the end of this section).

The EAKF algorithm is employed in this study and its implementation in WRF/DART follows the two-step approach of Anderson (2003), which updates the observation-space ensembles in the first step and then is followed by a regression step to update the model-space ensembles from the observation-space ensembles. The appendix derives the vector-matrix form of Eq. (6) of Anderson (2003), which expresses the EAKF as a regression. This has not been published elsewhere to the best of the authors' knowledge.

Like many other EnKF algorithms, the vector-matrix form of the EAKF equations (see the appendix) can be solved by serially assimilating observations in any order as long as the observation error covariance matrix is diagonal (Parrish and Cohn 1985), a common assumption in operational centers. Therefore, only one single observation is assimilated at a time. Anderson and Collins (2007) developed a scalable parallel algorithm, in which the observation prior ensembles are computed in parallel all at once at the beginning of assimilation, rather than serially after intermediate state updates. The key modification in the parallel algorithm is to adopt a joint state-observation space approach, in which the observation prior ensembles are updated exactly like the state variables.

A finite ensemble leads to sampling errors when computing the statistical relationship (covariance) between an observation and a state variable (or another observation). The sampling error, along with other error sources, tends to produce a systematic underestimate of ensemble variance that can result in poor filter performance or filter divergence. Two common methods to reduce this tendency are covariance localization and multiplicative inflation. In covariance localization, the covariance is multiplied by a localization factor $\rho(d)$ (separately in the horizontal and vertical) where d is the physical distance between an observation and a state variable (or another observation). In this study, $\rho(d)$ is the compactly supported correction function of Gaspari and Cohn (1999) with half-width c. For $d \geq 2c$, the observation has no impact on the state variable. For $d < 2c$, ρ approximates a Gaussian. In multiplicative inflation, the deviations of prior ensembles about the mean are multiplied by a factor greater than or equal to 1 immediately before the forward observation operator is applied for computing prior observation ensembles. The DART implemented an adaptive covariance inflation scheme that allows spatially and temporally varying inflation (Anderson 2009).

3. Radiance assimilation with an EnKF

Many satellite instruments measure radiation at the top of atmosphere (TOA) emitted by the earth–atmosphere system. TOA radiation is usually observed in different electromagnetic spectral bands (channels) in the quantity of radiance or brightness temperature. Remotely sensed radiance observations are sensitive to earth surface characteristics and several atmospheric variables (temperature, humidity, clouds, and precipitation, etc.) within a broad layer through radiative transfer equations (Liou 2002).

For assimilating radiance data within the EnKF described in section 2, the Community Radiative Transfer Model (CRTM; Han et al. 2006; Liu and Weng 2006) built in the WRF's DA (WRFDA; Barker et al. 2012) system is used as the radiance forward operator for computing radiance prior ensembles. The same strategy of using forward operators from a variational DA system was also adopted in other studies (e.g., Houtekamer et al. 2005; Hamill et al. 2011a,b; SLCH) to assimilate radiances (and other observations) within EnKF systems. In contrast to SLCH, where the prior ensembles of all observation types (including radiances) were computed from the WRFDA system, in this study only radiance prior ensembles come from WRFDA's forward operators and the prior ensembles of all other observation types are computed using the DART built-in forward operators to make use of observations from an existing WRF/DART experiment.

Like other observations, covariance localization is needed to reduce the sampling error for radiances, and the distance-based localization employed here requires an observation to have a defined location. But, radiance observations have no explicitly defined vertical locations owing to the nonlocal nature of the measurements. Houtekamer et al. (2005) assigned fixed pressure levels that corresponded to the approximate peaks of the AMSU-A weighting functions as the vertical locations. This approach was followed by Hamill et al. (2011a,b) but with the flow-dependent weighting functions and also applied to instruments other than AMSU-A. The Japan Meteorological Agency (JMA) uses the flow-dependent normalized weighting function itself to define the localization function in their global LETKF system, as proposed by Miyoshi and Sato (2007) and followed by Miyoshi et al. (2010). At the time of this work, the DART uses the same localization function (section 2) for all observation types. To fit the DART framework, we adopt the same vertical localization approach employed by Hamill et al. (2011a, b) and SLCH (i.e., use the peak levels of the flow-dependent weighting functions as they vary geographically and temporally).

The AMSU-A is a cross-track, line-scanned microwave sensor of 15 channels whose primary goal is the retrieval of temperature profiles. It has a 2343-km swath width and measures 30 pixels each swath with a ~48-km diameter footprint at nadir. In this study only a subset of temperature-sensitive AMSU-A channels are assimilated. Channels 1–4 and 15 were not assimilated here because of their large sensitivities to uncertain surface parameters (emissivity and skin temperature). The 20-hPa model top (see section 5) also prevents high peaking channels from being assimilated. Therefore, only channels 5–7 were assimilated, which correspond to weighting functions peaking around 700, 400, and 250 hPa, respectively.

Radiances are prone to systematic errors (i.e., biases) that must be corrected before they are assimilated. The radiance bias is often expressed by a linear combination of "predictors," which leads to a modified forward operator ($\tilde{H}$),

$$\tilde{H}(\mathbf{x}, \boldsymbol{\beta}) = H(\mathbf{x}) + \beta_0 + \sum_{i=1}^{N_p} \beta_i p_i, \qquad (1)$$

where H is the original forward operator (before bias correction); $\mathbf{x}$ is the model state vector; β_0 is a constant component of total bias; and p_i and β_i are the ith of N_p

predictors and corresponding bias-correction coefficients, respectively. Predictors can be separated into those related to the model state, such as surface temperature and layer thickness, and those related to the measurement, such as scan position (Eyre 1992). The bias-correction coefficients $\boldsymbol{\beta}$ are usually assumed channel dependent and can be estimated offline (Harris and Kelly 2001) or updated adaptively within a variational minimization process by including them in the state (Derber and Wu 1998). The latter method is referred to as variational bias correction (VarBC; Dee 2004).

The EnKF can use radiance bias correction produced by a variational DA system (e.g., Houtekamer et al. 2005; Miyoshi and Sato 2007; Buehner et al. 2010b) without additional cost if operational centers run variational- and ensemble-based DA systems simultaneously, as at the Canadian Meteorological Centre (CMC). Fertig et al. (2009) proposed and tested in an idealized setting an adaptive bias-correction method within a LETKF scheme by augmenting the state vector of each member with the bias-correction coefficients. Aravéquia et al. (2011) evaluated this ensemble bias-correction strategy with real observations. Alternatively, Miyoshi et al. (2010) and Hamill et al. (2011a) used the ensemble mean analysis to adaptively update deterministic bias-correction coefficients within the EnKF. SLCH used constant bias-correction coefficients ($\boldsymbol{\beta}$) generated by the VarBC from cycling WRFDA for one week.

Here we employ a simpler approach and run WRFDA's VarBC in an ''offline'' mode, in which the background term and all nonradiance observations are excluded. Therefore, the variational cost function J is reduced to

$$J(\boldsymbol{\beta}) = \frac{1}{2}(\boldsymbol{\beta} - \boldsymbol{\beta}_b)^{\mathrm{T}}\mathbf{B}_\beta(\boldsymbol{\beta} - \boldsymbol{\beta}_b) + \frac{1}{2}[\mathbf{y} - \tilde{H}(\mathbf{x}_r, \boldsymbol{\beta})]^{\mathrm{T}} \times \mathbf{R}^{-1}[\mathbf{y} - \tilde{H}(\mathbf{x}_r, \boldsymbol{\beta})], \tag{2}$$

where $\mathbf{y}$ is the observations; $\mathbf{R}$ is the observation error covariance matrix; $\mathbf{x}_r$ is a reference field and considered unbiased; and $\boldsymbol{\beta}_b$ and $\mathbf{B}_\beta$ are the background bias-correction coefficient vector and the associated error covariance, respectively. The $\boldsymbol{\beta}$ can be easily obtained with few iterations of the minimization algorithm for this linear problem. Similar to SLCH, the ''spunup'' $\boldsymbol{\beta}$ at the end of the offline update cycles is held fixed in the EnKF assimilation for the entire experimental period. Note that if the reference field is taken from the EnKF ensemble mean analysis and $\boldsymbol{\beta}$ is updated adaptively with $\boldsymbol{\beta}_b$ from the previous analysis cycle, this offline ''VarBC'' mode is identical to that proposed by Miyoshi et al. (2010).

To implement this approach, we choose the National Centers for Environmental Prediction (NCEP) operational global analysis, which assimilates radiances from many satellite sensors, as the reference field. The predictors of Eq. (1) used in the WRFDA VarBC include seven parameters: the scan position, the square and cube of scan position, 1000–300- and 200–50-hPa layer thicknesses, surface skin temperature, and total column water vapor, which are similar to those used in the European Centre for Medium-Range Weather Forecasts (ECMWF) global analysis. Here $\mathbf{B}_\beta$ is a diagonal matrix, with the variance values σ^2/N on the diagonal controlling the adaptivity of a specific predictor coefficient for a specific radiance channel, where σ^2 is an estimate of the radiance error variance for the associated channel. As explained in Dee (2004), this means that the weight given to the background parameter estimate is equivalent to that of N additional radiance observations. In the ECMWF global DA system, N is set to 10^4 (Dee and Uppala 2009). In this regional DA setting, we take a smaller value, 5000, to give more weight to the latest observations.

Liu et al. (2011) demonstrated over an Arctic-centered domain that a month-long offline WRFDA VarBC run is necessary to obtain stable bias-correction coefficients. Poli et al. (2010) also reported slow adjustment (up to two months) of radiance bias correction due to the removal of global positioning system (GPS) radio occultation (GPSRO) data in the ECMWF global DA system. In this study, we ran WRFDA offline VarBC mode over the computational domain for a three-month (May–July 2008) period prior to the EnKF assimilation to obtain a set of spunup bias-correction coefficients.

The usual practice with an EnKF would be to apply the forward operator $\tilde{H}$ given by Eq. (1) to each member to obtain bias-corrected radiance prior ensembles, with no adjustment of the raw radiance observations. However, we found that the ensemble spread of bias correction was usually small $[O(10^{-1})]$ relative to the ensemble spread in brightness temperature. Thus, we neglect the spread in bias correction and take the predictors $\mathbf{p}$ from the prior ensemble mean; that is, bias correction is based on the ensemble mean only and is not specific to each member. This greatly simplifies the observation handling, as we can adjust the raw radiance observations while keeping the radiance prior ensembles uncorrected.

We follow SLCH and adopt radiance quality-control (QC) procedures in WRFDA that consist of numerous checks to ensure that only ''good'' radiance observations are assimilated. The AMSU-A QC procedures include checks on (i) gross values, which removes observations with brightness temperatures smaller than 150 K or larger than 450 K; (ii) observing geometry, which removes three pixels with large scan angles on the swath

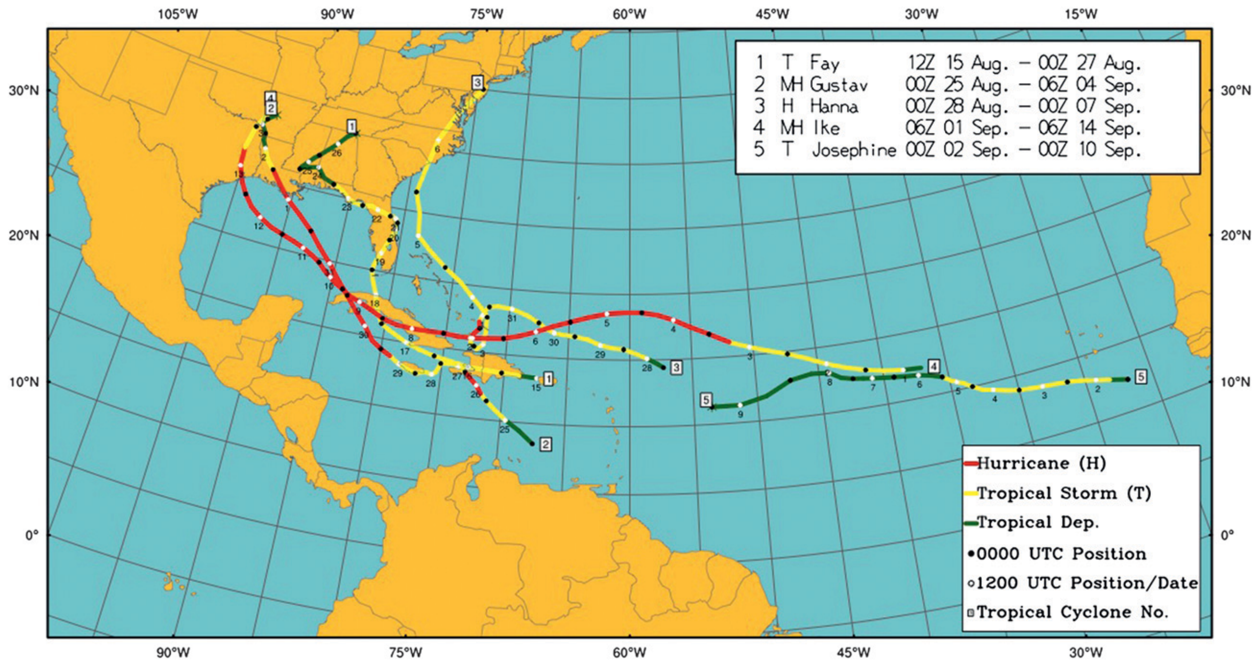

FIG. 1. NHC best track for the five named storms during 11 Aug–13 Sep 2008. See legend for meanings of colors and symbols used in the depictions of tracks.

edges; (iii) surface types, which removes pixels with mixed surface types; and (iv) weather conditions, which removes observations over precipitating pixels. These checks are applied to each member and the observation is rejected if any member fails any check. In SLCH, an ''outlier'' test was also performed within WRFDA, where a radiance observation was rejected if the bias-corrected innovation (observation minus prior) exceeded $3\boldsymbol{\sigma}_o$, where $\boldsymbol{\sigma}_o$ is the observation error standard deviation. However, here the outlier check is performed within the EnKF using the prior ensemble mean $\overline{\mathbf{y}_b} = \overline{H(\mathbf{x}_b)}$ and ensemble variance $\boldsymbol{\sigma}_b^2$ for each observation $\mathbf{y}_o$. The observations were rejected when $|\mathbf{y}_o - \overline{\mathbf{y}_b}| > 3\sqrt{\boldsymbol{\sigma}_b^2 + \boldsymbol{\sigma}_o^2}$. The above QC checks, together with a 72-km thinning mesh, reject ~70% of the total radiance observations over the computational domain.

4. Overview of tropical cyclone cases

Before describing the EnKF experiments, a brief overview of the five named storms (Fay, Gustav, Hanna, Ike, and Josephine) is provided. Figure 1 shows the National Hurricane Center (NHC) best tracks of the storms. Among the five, Fay and Josephine were tropical storms, Hanna became a hurricane, and Gustav and Ike reached major hurricane status and had at least one rapid-intensification period. All storms except Josephine made landfall. The lifetime of the storms ranged from 8 days (Josephine) to 13 days (Ike). This period was devastating for Haiti, where over 800 people were killed by four consecutive storms (Fay, Gustav, Hanna, and Ike). Ike was the most destructive and strongest storm of the 2008 hurricane season, devastating Cuba as a major hurricane and later making landfall near Galveston, Texas, at category 2 (nearly category 3) intensity. As it zigzagged from water to land, Fay became the first storm in recorded history to make landfall in Florida 4 times.

5. Experimental setup

To test the assimilation of AMSU-A radiances with WRF/DART, we performed cycled forecast-analysis experiments for the period 0000 UTC 11 August, some four days before Fay was declared a tropical depression, to 0000 UTC 13 September 2008, after Ike's landfall. The model domain (Fig. 2) covers the track of all five storms during this period. In the two principal experiments, WRF/DART assimilated either a control set of observations that excluded satellite radiances or the control observations plus AMSU-A radiances. Here, we document the details of those experiments.

All forecasts employ version 3.2.1 of the Advanced Research WRF Model (ARW-WRF, hereafter WRF; Skamarock et al. 2008). In all experiments, the horizontal grid spacing is 36 km, there are 45 vertical levels

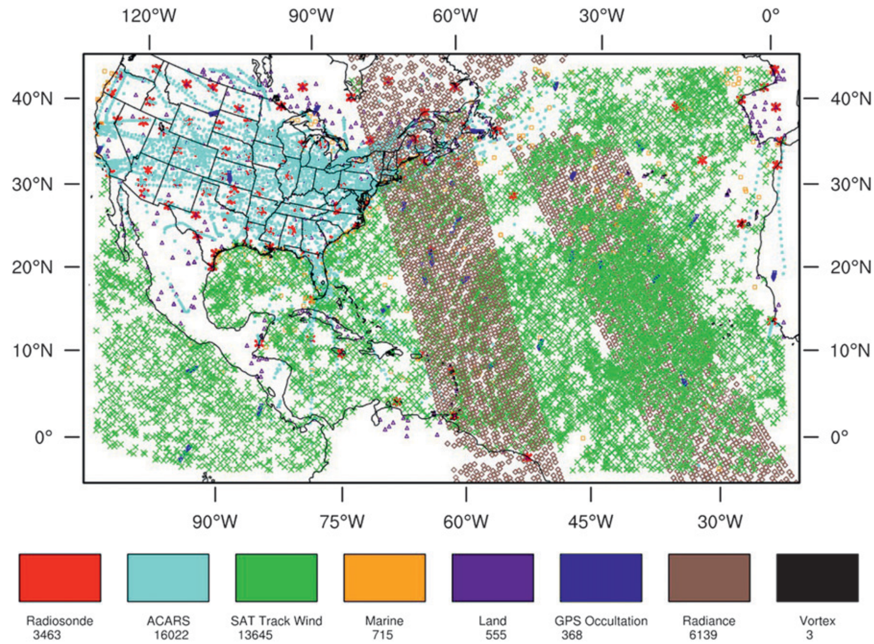

FIG. 2. Snapshot of observations assimilated at 0000 UTC 16 Aug 2008.

up to the model top at 20 hPa, and the following parameterizations are used: the WRF Single-Moment 5-Class Microphysics scheme (WSM5; Hong et al. 2004); the Goddard shortwave (Chou and Suarez 1994) and Rapid Radiative Transfer Model (RRTM) longwave (Mlawer et al. 1997) radiation schemes, including the refined upper boundary condition for RRTM (Cavallo et al. 2011) that is necessary when cycling with model tops above 50 hPa; the Yonsei University (YSU) boundary layer scheme (Hong et al. 2006); the Noah land surface model (Chen and Dudhia 2001); and the Kain–Fritsch cumulus parameterization (Kain and Fritsch 1990).

The WRF/DART assimilation system consists of the EAKF implemented in DART and WRF-specific interfaces, observation operators, and observation-processing tools. Overall, the system configuration follows Torn (2010). There were 96 ensemble members in all experiments. Two other important aspects are the covariance localization, which greatly reduces the detrimental effects of sampling error in the assimilation, and the multiplicative inflation, which counteracts the tendency for the ensemble forecasts to have too little spread owing especially to sampling error and unrepresented model error. The maximum half-width c of the covariance localization function (see section 2) is set to 1000 km in the horizontal and 12.8 km in the vertical, but is adaptively reduced at each analysis time where observations are dense. For typical observation coverage in this study, c varies between ~320 and ~1000 km in the horizontal and ~3.9 and ~12.8 km in the vertical. The multiplicative inflation is calculated separately for each element of the state vector with the adaptive technique of Anderson (2009), assuming a prior standard deviation of 0.6 in the update of the inflation and reducing the deviation of the inflation from one by 10% before each update.

In the cycling system, ensemble analyses are generated every 6 h (at 0000, 0600, 1200, and 1800 UTC). The 6-h ensemble forecasts require an ensemble of lateral boundary conditions; we take their mean to be the 6-h forecast from NCEP's Global Forecast System (GFS) and construct the deviations about that mean following Torn et al. (2006) by using WRFDA to generate realizations of spatially correlated, balanced noise whose covariance is specified by the WRFDA background-error covariance. The initial ensemble at 0000 UTC 11 August has mean equal to the GFS analysis at that time and perturbations constructed similarly to those for the lateral boundary conditions. Additionally, a deterministic 72-h WRF forecast was initialized from the 0000 and 1200 UTC ensemble-mean analyses, with lateral boundary conditions also taken from the appropriate GFS forecasts. These deterministic forecasts are used for the verification statistics shown later in section 6.

Two parallel experiments using 96-member ensembles were configured to evaluate the impact of assimilating AMSU-A radiances with an EnKF on the forecasts of Atlantic TCs. The first experiment (hereafter ''NoAMA'') assimilated conventional observations from radiosondes, aircraft, satellite-derived winds, and land and oceanic surface stations, together with GPS dropwindsonde observations released from the National Oceanic and Atmospheric Administration (NOAA) G-IV aircraft in the synoptic environment surrounding TCs (e.g., Aberson 2010) and GPS refractivity observations from the Constellation Observing System for Meteorology Ionosphere and Climate (COSMIC; Liu et al. 2007). The preprocessing of the conventional observations followed Torn and Hakim (2008); in particular, both aircraft and satellite winds are averaged over volumes of 36 km by 36 km horizontally and 25 hPa vertically. The NoAMA experiment also assimilates storm position and intensity as in Chen and Snyder (2007), where the latitude, longitude, and minimum sea level pressure are taken from NHC advisories and the model-predicted storm position is diagnosed from the location of maximum 850-hPa circulation as in Cavallo et al. (2013).

The second experiment (hereafter ''AMA'') assimilated all observations from NoAMA, but also included AMSU-A radiances from *NOAA-18* and *METOP-2* satellites, using the procedure outlined in section 3. The raw radiance data were thinned on a 72-km grid to avoid potential correlations between adjacent observations (Liu and Rabier 2002). In both experiments, observations within ± 1.5 h of the analysis times were assimilated and all observations were assumed to be valid at the analysis times. In WRF/DART, the main observation QC is the innovation check as described in section 3. Figure 2 shows a snapshot of observations assimilated at 0000 UTC 16 August. Clearly, satellite-derived winds and radiances are the two major data sources over the Atlantic Ocean.

6. Results

The TC track and intensity forecast performance from the two experiments was evaluated by comparing model output to the NHC best-track data. The environmental fields surrounding the TCs were assessed by comparing them to GPS dropwindsonde observations and ECMWF Re-Analysis Interim (ERA-Interim) reanalyses.

a. Single forecast verification

To provide examples of how assimilation of radiances affects the TC forecasts, Fig. 3 shows the 72-h forecast tracks of four TCs (Fay, Gustav, Hanna, and Ike) initialized about 3 days before their landfalls in the United States for the experiments AMA (open circle) and NoAMA (filled circle). The best-track positions (star) are also plotted. The vortex positions at the initial times from both experiments are very close to the best-track locations, which was noted for almost the whole experimental period (not shown) and is likely related to the assimilation of NHC advisory vortex positions.

Forecast track errors varied among the different TCs. The forecast track from the AMA experiment agreed more closely with the best track than the NoAMA experiment for Fay (initialized at 0000 UTC 16 August; Fig. 3a) and Gustav (initialized at 1200 UTC 29 August; Fig. 3b). The beneficial impact of assimilating AMSU-A radiances is more pronounced for Gustav, which rapidly intensified to a category-4 hurricane before it made landfall on the eastern coast of the Isle of Youth, Cuba, near 1800 UTC 30 August. The NoAMA experiment had a significant westward bias and slower vortex movement, missing the landfalls in Cuba late 30 August and Louisiana around 1500 UTC 1 September. The forecast track from AMA, however, passed over Cuba, even though it was slightly too far west and fast. At the end of the forecast (1200 UTC 1 September), 3 h before Gustav made landfall in Louisiana, the AMA's vortex position was in close agreement with the best track.

Forecast tracks for Hanna (initialized at 0000 UTC 3 September; Fig. 3c) and Ike (initialized at 1200 UTC 10 September; Fig. 3d) were similar between AMA and NoAMA. Both experiments reasonably forecasted Hanna's track, though the model storms moved too fast, making landfall ~6 h earlier and too far west. From the best track, Hanna moved southward in the first 6-h and then turned northeast, followed by a northwestward recurvature 12 h later. Both experiments missed the southward movement, contributing to faster northward movement and an earlier landfall.

The worst track forecast occurred for Ike, with a significant westward bias in both experiments. After examining Ike track forecasts initialized at other analysis times, we found that this left-of-track bias persisted beginning from the 0000 UTC 8 September analysis and was similar for both experiments. However, even in these poor forecasts, assimilating AMSU-A radiances did not degrade the track forecasts compared to the NoAMA experiment. Note that most global and regional operational models featured a similar persistent westward bias over the western Gulf of Mexico several days before Ike's landfall in Texas (see Berg 2009). Interestingly, Zhang et al. (2011) reported a much-improved track forecast of Ike using a convective-permitting EnKF system with the assimilation of airborne Doppler radar observations, and Wang (2011) demonstrated the ability of a hybrid variational/ensemble DA system to correct this westward bias.

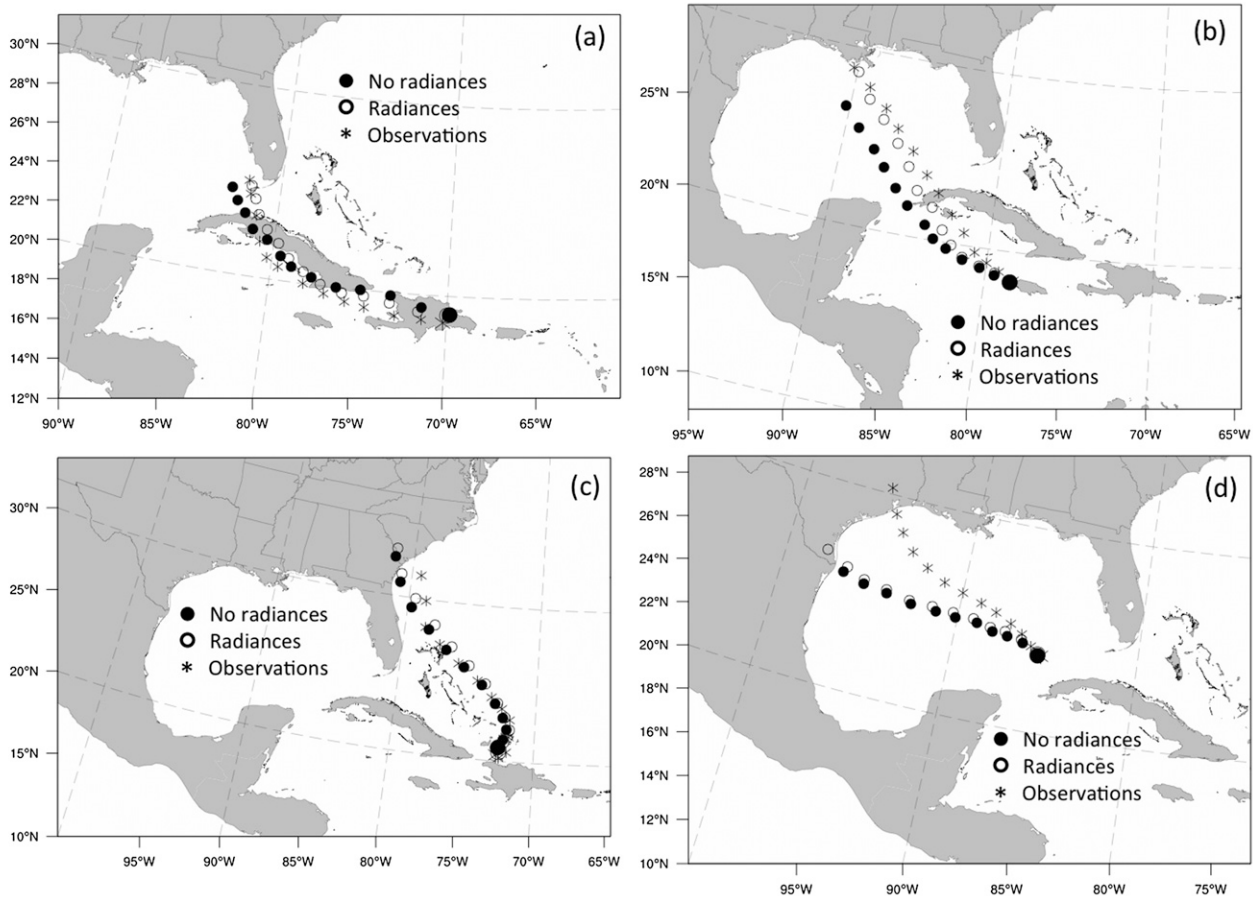

FIG. 3. Forecast tracks of 4 TCs initialized about 3 days before making landfall in the United States. (a) Fay: initialized at 0000 UTC 16 Aug and landfall near Key West, Florida, at 2030 UTC 18 Aug; (b) Gustav: initialized at 1200 UTC 29 Aug and landfall near Cocodrie, Louisiana, at 1500 UTC 1 Sep; (c) Hanna: initialized at 0000 UTC 3 Sep and landfall near North Carolina/South Carolina border at 0720 UTC 6 Sep; (d) Ike: initialized at 1200 UTC 10 Sep and landfall at north end of Galveston Island, Texas, at 0700 UTC 13 Sep.

b. Accumulated track and intensity error statistics

Figure 4 shows the mean absolute track errors of the two experiments from the analysis to 72-h forecast lead times for the lifetime of each TC. Sample sizes for each lead time are also displayed in the plots. To ensure a homogeneous comparison between the two experiments, a forecast is used in the statistics only if both experiments diagnosed the existence of a TC. The overall track-error reduction due to radiance assimilation is evident for all five TCs. For Fay, nearly uniform improvement (~30 km smaller track error) is achieved beyond 24 h. A slight degradation for short lead times (<24 h) occurs for Gustav, Ike, and Josephine when radiances are assimilated. However, radiance DA improves the track forecasts beyond 48 h. The relative track error reduction at 72 h (48 h for Josephine) varies from ~10% for Hanna and Josephine to ~35% for Gustav.

Figure 5 shows the mean absolute error averaged over all storms as a function of forecast lead time for track, maximum 10-m wind speed, and minimum sea level pressure (SLP). Statistical significance of the error difference between the two experiments was assessed by applying a bootstrap resampling technique (Hamill 1999). Specifically, the difference between the experiments' errors was calculated for each forecast. Random samples (with replacement) were drawn from the distribution of differences for each forecast hour, and the mean difference was calculated. This process was repeated 10 000 times. The 90% confidence interval for the average difference between the two experiments was estimated from the distribution of the resampled mean differences. If zero was not contained within the bounds of the confidence interval, then the difference between the experiments' errors was statistically significant at the 90% level.

The gain by assimilating AMSU-A radiances is evident for both track and intensity forecasts, particularly beyond 48 h. Lower track errors of the AMA experiment are statistically significant from 36 to 72 h. The

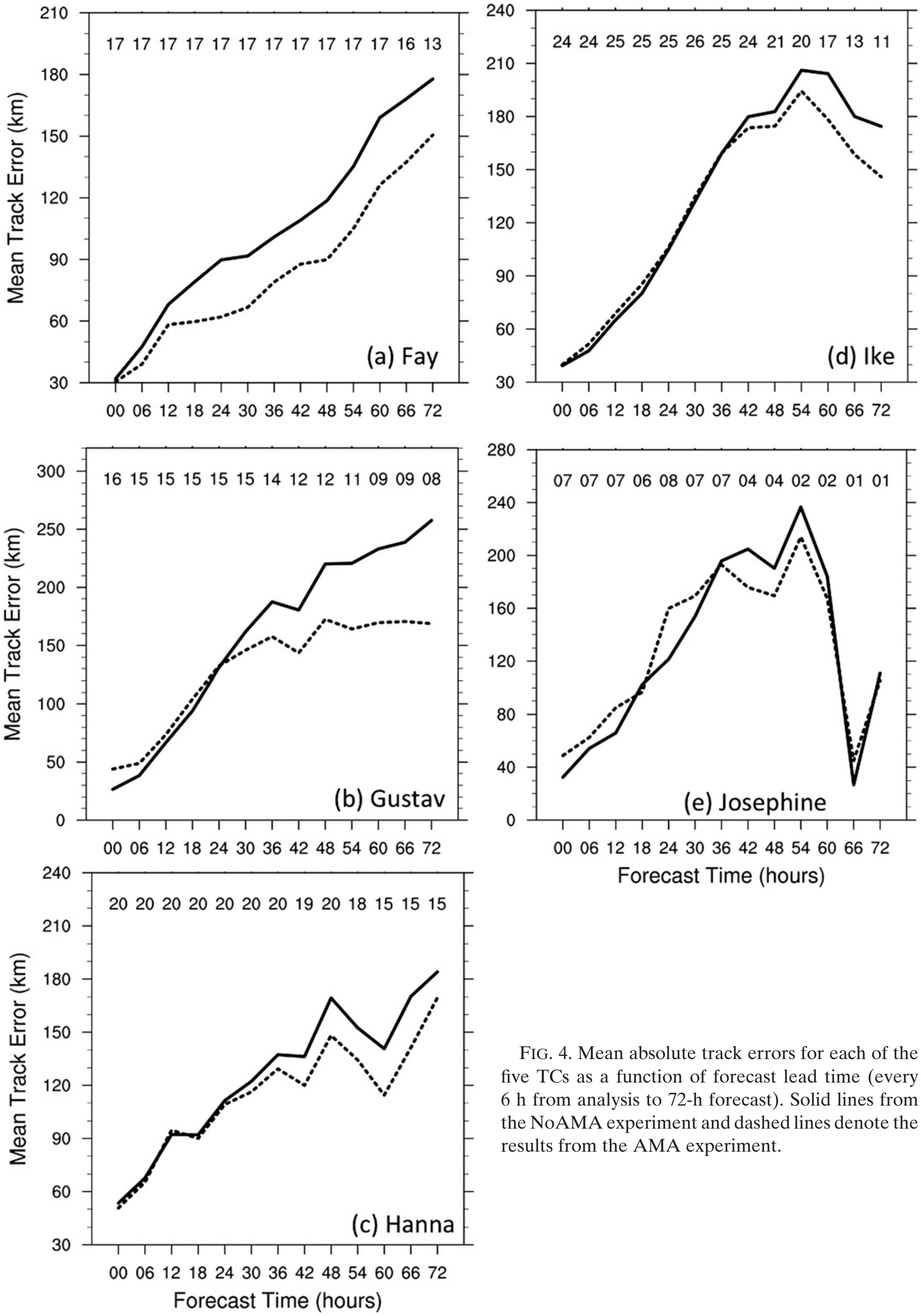

FIG. 4. Mean absolute track errors for each of the five TCs as a function of forecast lead time (every 6 h from analysis to 72-h forecast). Solid lines from the NoAMA experiment and dashed lines denote the results from the AMA experiment.

track error is reduced by ~16% from 48 to 72 h. The improvement of maximum wind speed forecasts is limited, while for minimum SLP, assimilating AMSU-A yields a ~13%–20% reduction of SLP errors from 48 to 72 h that is statistically significant and consistent with SLCH. Radiance DA also led to a statistically significant increase of error at the analysis time, despite the improvement evident at 48 h and beyond.

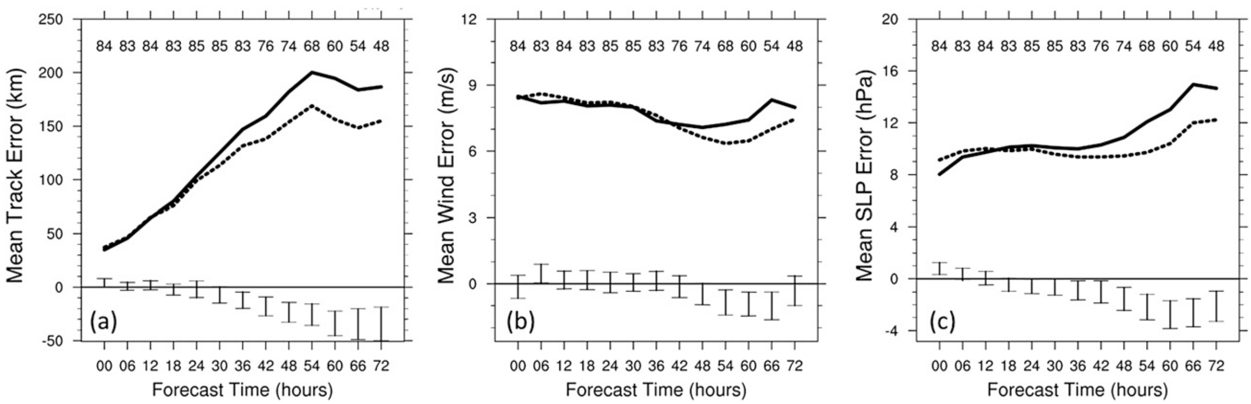

FIG. 5. Mean absolute errors as a function of forecast lead time for (a) track, (b) maximum wind speed, and (c) minimum sea level pressure for all storms. Solid lines denote the results from the NoAMA experiment and dashed lines denote the results from the AMA experiment. Bounds of the 90% confidence interval based upon differences between the two experiments' errors (see section 6b) are also shown.

The AMA experiment tends to produce weaker low pressures and lower maximum wind speeds than the NoAMA experiment (not shown). This is likely attributed to the large AMSU-A footprint that varies from ~48 km × 48 km at nadir to ~80 km × 150 km at limb (Bennartz 2000), and more investigation is needed to understand this. Despite encouraging results regarding the TC intensity forecast improvement, intensity errors remain large because of coarse (36 km) model resolution used for the forecast. Similar results were also found by Torn (2010), who showed a pronounced weak bias for most intense storms. We expect that more realistic intensity forecasts can be achieved by increasing model resolution (Davis et al. 2010; Cavallo et al. 2013).

c. *Forecast verification against dropwindsonde observations*

Recall that the current system is incapable of assimilating rain-affected microwave radiances, and the QC procedure prohibits the use of AMSU-A data in the precipitating TC core area. Thus, the improved track forecasts by assimilating AMSU-A radiances are likely due to a better depiction of large-scale environmental flow in the analyses and subsequent forecasts. To test this hypothesis, we verified the forecasts against GPS dropwindsonde observations released from NOAA G-IV aircraft (Aberson 2010). The G-IV dropwindsondes sample the atmosphere below flight level (near 150 hPa) at 150–200-km horizontal intervals. G-IV dropwindsondes were deployed in the synoptic environments surrounding the storms and did not penetrate the inner cores of TCs, making the dropwindsondes an ideal data source to evaluate the environmental fields from the two experiments.

Figure 6 shows bias and root-mean-square error (RMSE) of 48-h forecasts verified against dropwindsonde observations taken within ±1.5 h of 0000 and 1200 UTC during the experimental period. The corresponding dropwindsonde distribution is provided in Fig. 7. A total of 208 dropwindsondes were collected for verification.

The AMA experiment agrees more closely with the dropwindsondes than the NoAMA experiment consistently for all variables (U, V, T, and Q), except for some degradation in terms of bias for V-wind component below 300 hPa and specific humidity at 850 hPa. The RMSE reduction for wind is nearly uniform at all levels and is greater than the error reduction for temperature and specific humidity. Note that AMSU-A channels measure atmospheric temperature, and the impact on the wind and moisture fields likely result from multivariate correlations implied in the EnKF analyses. The large wind impact from the assimilation of temperature-sensitive radiances is consistent with McNally (2007), who found that withholding the temperature information provided by AIRS retrievals significantly degraded the analyzed and short-range forecast wind fields at high-latitude regions.

d. *Comparison with ERA-Interim reanalyses*

To obtain more insight on the differences between the NoAMA and AMA experiments, the EnKF mean analyses were compared to the ECMWF's ERA-Interim reanalyses (Dee et al. 2011). ECMWF has produced operational TC forecasts since October 2004 (Van der Grijn et al. 2005) and is one of the best operational centers for TC track forecasts (Fiorino 2009). Therefore, ERA-Interim reanalyses (~79-km resolution) are assumed to be a good reference for the assessment of large-scale flow.

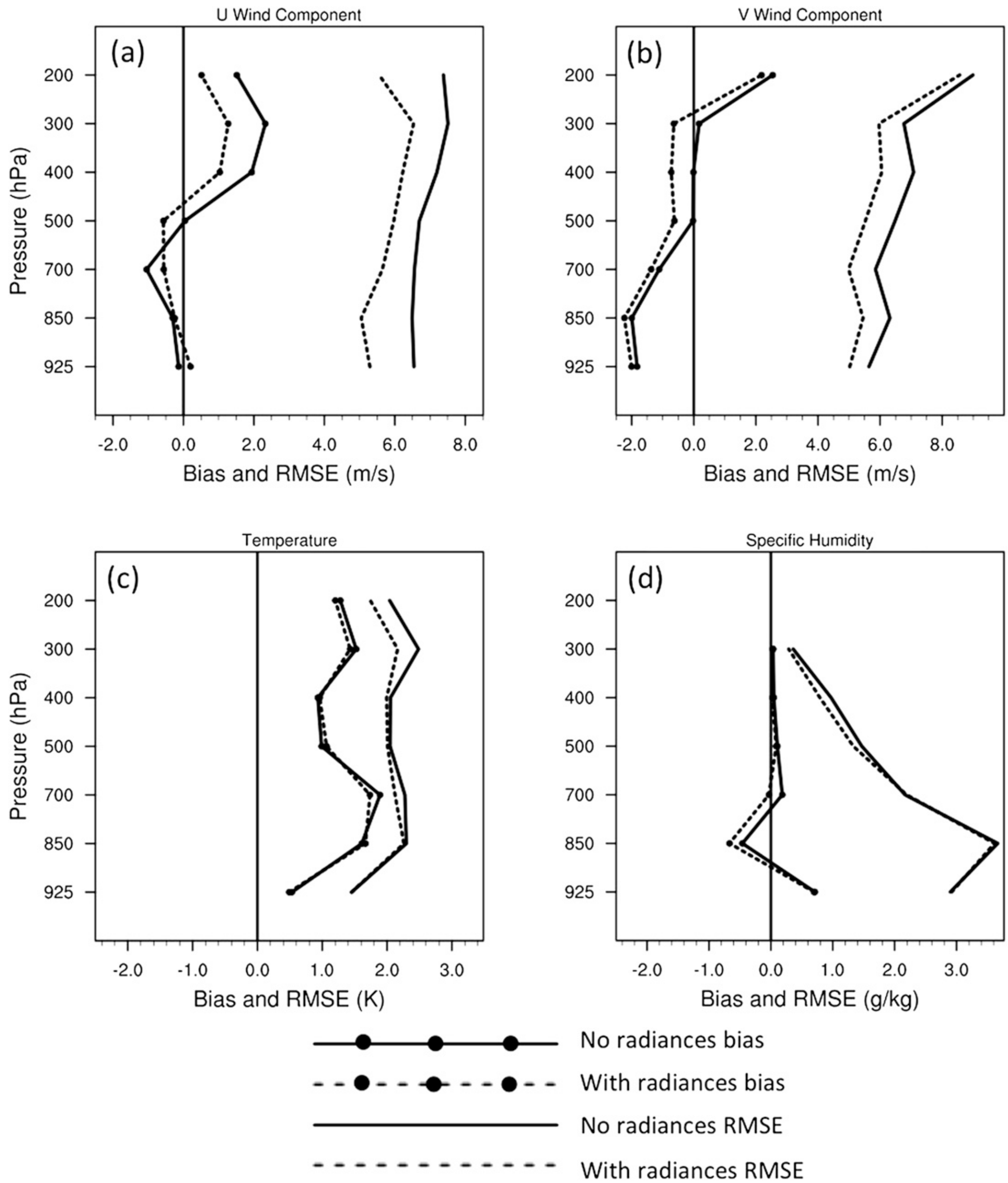

FIG. 6. Bias and RMSE of 48-h forecasts verified against dropwindsonde observations for the experiments with and without the assimilation of AMSU-A radiances.

The mean differences between the experiments' 0000 UTC analyses and corresponding ERA-Interim fields (model minus ERA-Interim) over the experimental period are displayed in Fig. 8 for 500-hPa temperature (left panels) and 250-hPa geopotential height (right panels). The NoAMA analyses exhibit significant warm biases (Fig. 8a) relative to the ERA-Interim over most of the domain, with bias values larger than 1 K in the Gulf of Mexico, Caribbean Sea, and off the west coast of Africa. Consistent with the warm bias at 500 hPa, the 250-hPa heights were generally higher than in the ERA-Interim analyses (Fig. 8b). Assimilating AMSU-A radiances resulted in a net cooling over the Atlantic Ocean, with both temperatures and heights (Figs. 8c,d) agreeing more closely with the ERA-Interim.

The mean analysis differences at 0000 UTC between the two experiments (AMA minus NoAMA) are shown in Fig. 9. Radiance DA clearly cooled temperatures over the Atlantic Ocean and lowered the heights, with an associated weakening of the flow around the subtropical

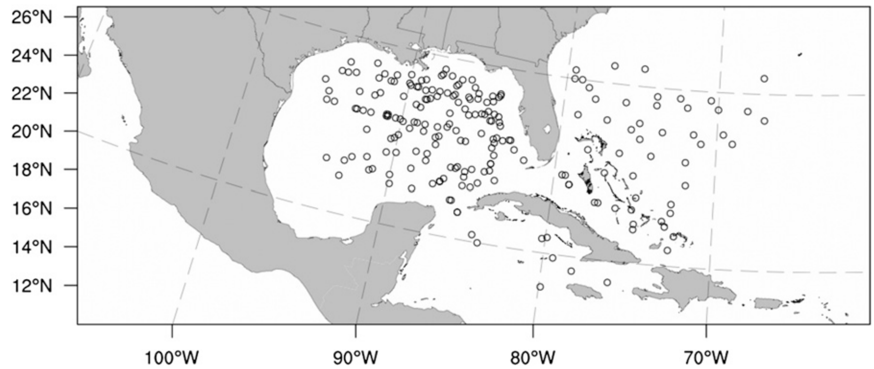

FIG. 7. Dropwindsonde distribution at 0000 and 1200 UTC used for the 48-h forecast verification in Fig. 6. A total of 208 dropwindsondes are available for verification.

high. This weaker steering flow in the AMA experiment is consistent with a synoptic pattern that would allow TCs to recurve to the northwest and north, as was observed in many TC tracks (see Fig. 3).

It is unclear whether the WRF or DA was the primary cause of this warm bias when radiances were not assimilated. We suspect that a WRF deficiency plays some role in the generation of the warm bias, as in

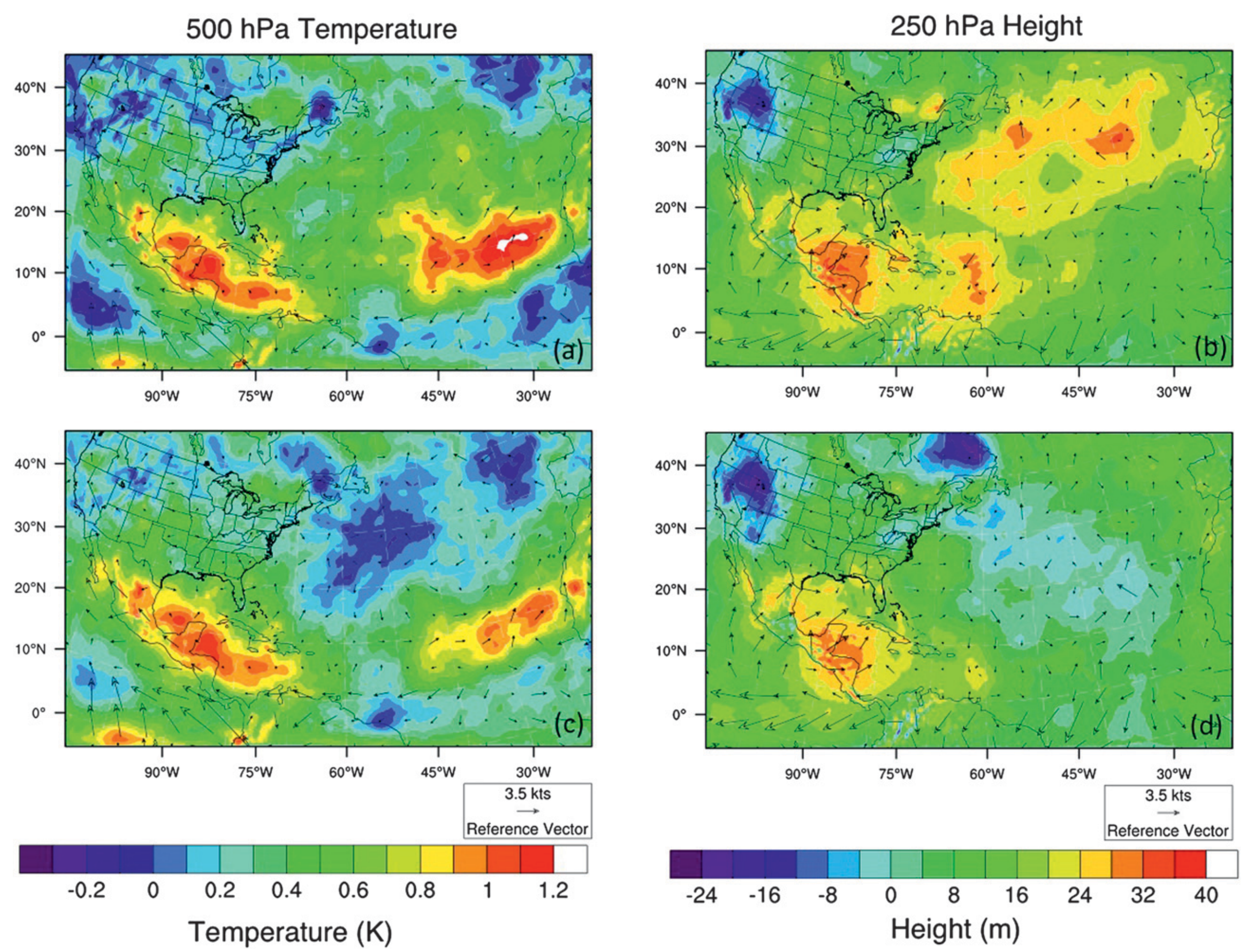

FIG. 8. Mean differences between the EnKF 0000 UTC analyses and corresponding ERA-Interim reanalysis fields (model minus ERA-Interim) over the experimental period for (a),(c) 500-hPa temperature and (b),(d) 250-hPa geopotential height. (a),(b) NoAMA experiment and (c),(d) AMA experiment.

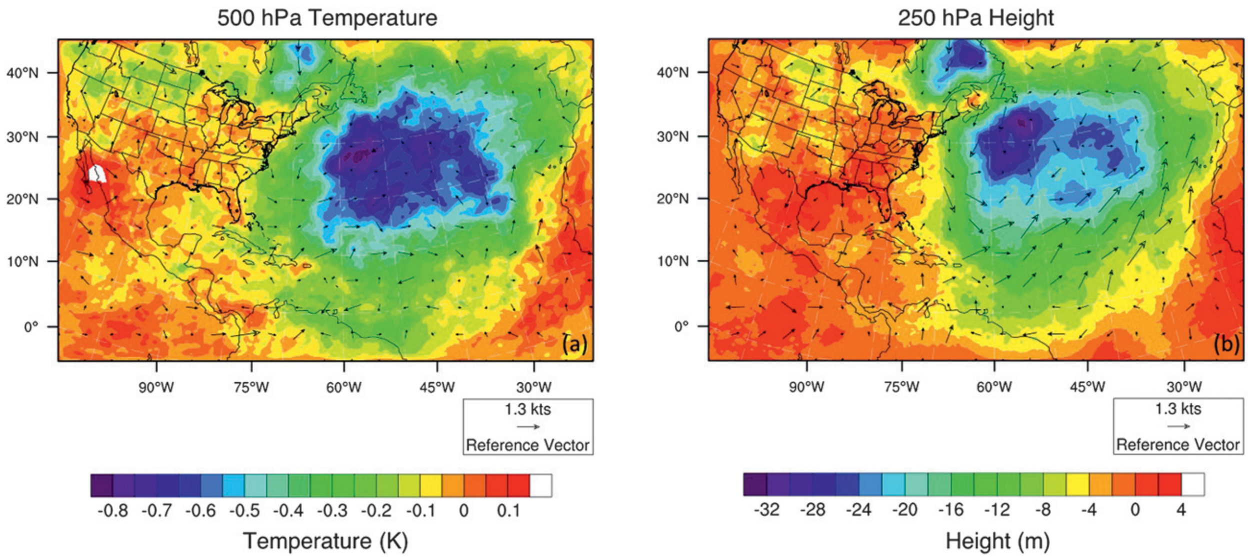

FIG. 9. As in Fig. 8, but for the mean 0000 UTC analysis differences between AMA and NoAMA (AMA minus NoAMA).

a similar setting of the EnKF for real-time TC forecasts, the magnitude of warm bias appeared to be sensitive to the choice of WRF cumulus parameterization scheme (R. Torn 2011, personal communication). At the ECMWF, the reformulation of convective entrainment in November 2007 resulted in the record-setting performance of TC track prediction in the 2008 season (Fiorino 2009).

e. Importance of synergistic assimilation of AMSU-A radiances and satellite winds

Radiances and satellite winds are the two major observations sets over the Atlantic Ocean (Fig. 2), measuring the temperature and wind fields, respectively. Two additional EnKF cycling experiments were conducted to evaluate the extent to which these observations are redundant or complementary for TC track prediction. In one experiment, denoted as "GTS," neither satellite winds nor AMSU-A radiances were assimilated. In another experiment, named "GTS+RAD," AMSU-A radiances were assimilated but not satellite winds. To ease the comparison for four experiments, the experiments NoAMA and AMA are renamed as "GTS+SAT" (i.e., include satellite winds, but not AMSU-A radiances) and "GTS+SAT+RAD" (i.e., include both satellite winds and AMSU-A radiances), respectively. The WRF and EnKF configurations are identical for all four experiments.

Figure 10 displays the absolute mean track errors as a function of forecast lead time for the four experiments. Compared to Fig. 5a, the sample sizes in the track error statistics are smaller, because the GTS experiment (no DA of satellite winds or AMSU-A radiances) overall missed more TCs (Fig. 11) in the forecasts and the other three experiments' sample sizes were adjusted downward to ensure a homogeneous comparison. However, the track error curves in Fig. 10 for GTS+SAT and

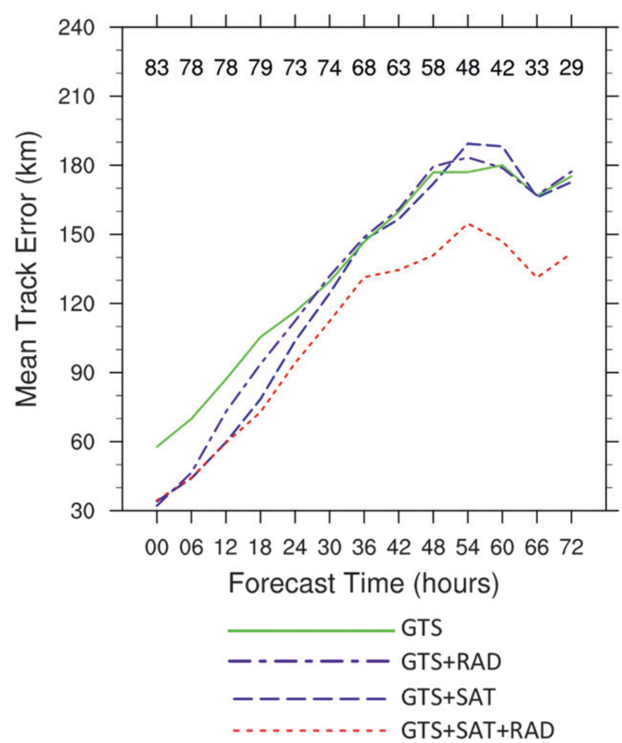

FIG. 10. As in Fig. 5a, but for the comparison of four experiments (see section 6e).

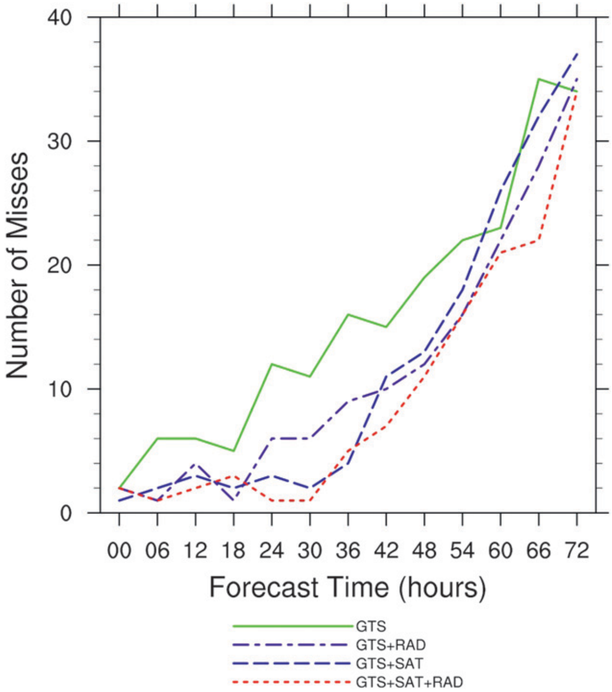

FIG. 11. As in Fig. 10, but for the number of missed storms for four experiments.

GTS+SAT+RAD (i.e., previous NoAMA and AMA) are very similar to those in Fig. 5a, even though larger samples were used in the latter. Moreover, satellite winds appear to have a larger positive impact than AMSU-A radiances within 30 h. The smaller radiance impact in the short range could likely be overcome by adding more sensors from more satellites. The track errors are comparable beyond 36 h for the GTS, GTS+SAT, and GTS+RAD experiments. The most remarkable observation is that assimilating both satellite winds and AMSU-A radiances in the experiment GTS+SAT+RAD produced the lowest track errors for nearly all forecast ranges and especially beyond 36 h. This may imply that the synergistic assimilation of thermal and wind observations is crucial to obtain well-balanced mass and wind fields in the TC environments, thus, maximizing the benefits of assimilating both observation types for medium-range TC track forecasts. Hartung et al. (2011) also found that the best forecasts for a midlatitude extratropical cyclone were obtained when both wind and temperature observations were assimilated.

Figure 11 shows the number of missed storms for the four experiments. It is apparently overall consistent with Fig. 10; that is, larger track errors in Fig. 10 correspond to more misses in Fig. 11. Comparing the sample sizes in Figs. 5a and 10 with the number of misses in Fig. 11 reveals an apparent inconsistency. For instance, the number of misses at 72 h is similar (~34–37) for all experiments, but the sample sizes (i.e., number of storms caught) in Figs. 5a and 10 are substantially different at 72 h. The reason is that the different experiments miss different storms, and a homogeneous comparison is taken into account in the sample size counting. To see if the conclusions drawn from Fig. 10 are sensitive to the cases used in the track error statistics, we additionally compared the track errors between two-pair experiments: GTS+RAD versus GTS+SAT and GTS+RAD versus GTS+SAT+RAD, while following the same rule for homogeneous comparison. We obtained the same indication as in Fig. 10 (not shown).

7. Summary and future perspectives

This study further enhanced the radiance DA capability developed by SLCH within an EnKF system. The QC procedure and bias-correction strategy were revised to better use radiance data. The updated EnKF system also allows a blended use of externally computed forward operators for radiances and internally calculated forward operators for other observation types. Moreover, the impact of assimilating AMSU-A radiances from the *NOAA-18* and *METOP-2* satellites on Atlantic TC forecasts was evaluated thoroughly during a month-long experimental period when five TCs formed.

The environmental fields surrounding the storms agreed more closely with dropwindsonde observations and ECMWF ERA-Interim reanalyses when assimilating AMSU-A radiances in addition to nonradiance observations. More specifically, both analyses and forecasts had a tropospheric warm bias over much of the domain when no radiances were assimilated, but assimilating AMSU-A radiances reduced the warm bias over a large portion of the Atlantic. Furthermore, the RMSE reduction appeared to be more pronounced for environmental wind fields than temperature and moisture fields with the assimilation of temperature-sensitive AMSU-A channels, consistent with McNally (2007).

The better depiction of environmental flow by assimilating AMSU-A radiances likely contributed to the substantially more accurate TC track predictions, particularly for forecast ranges beyond 36 h with the overall track error reduction up to 16%. A similar error reduction also occurred for intensity forecasts both in terms of maximum wind speed and minimum SLP, consistent with SLCH. However, TC intensity still remains too weak because of the use of coarse resolution (36 km) in the WRF forecasts. Another important finding is that AMSU-A radiances apparently have to be assimilated together with satellite winds to maximize the benefit on the TC track forecast.

Radiance assimilation within the EnKF is still in its infancy even though a number of studies have focused on this topic and some NWP centers have already assimilated radiances in operational EnKF systems. More efforts are needed for the optimal use of radiance data. In this study, during the whole experiment period we applied a set of fixed radiance bias-correction coefficients that were obtained through offline statistics generated over a 3-month spinup period. Satisfactory results were achieved with this simple bias-correction strategy. Nevertheless, more practical strategies of radiance bias correction can be easily implemented in the same framework as our offline statistics. For example, we can adaptively update, during the cycling EnKF, bias-correction coefficients using the EnKF mean analyses or other global analyses as reference fields. Different bias-correction strategies will be assessed in future studies.

Another important aspect is radiance vertical covariance localization. Current observation space covariance localization method in the EnKF, which uses either the peaks of channels' weighting functions or the full weighting functions to define the vertical localization function, may lead to suboptimal assimilation of radiance channels sensitive to both temperature and moisture, and could be more problematic for assimilating cloud/precipitation-affected radiances (e.g., Otkin 2012). Alternatively, the hybrid variational/ensemble technique (e.g., Lorenc 2003; Wang et al. 2008) uses model space covariance localization, which was proven more suitable than observation space covariance localization in the EnKF for radiance vertical localization (Campbell et al. 2010).

We plan to assimilate more radiance data from both microwave and infrared sensors and test different bias-correction and vertical covariance localization strategies using both pure ensemble Kalman filters and hybrid DA techniques in future work.

Acknowledgments. We are grateful to the Air Force Weather Agency for funding this work.

APPENDIX

Vector-Matrix Derivation of Ensemble Adjustment Kalman Filter

We want to show that the scalar-form regression Eq. (6) in Anderson (2003) can be written in full vector-matrix form. The two-step EAKF algorithm begins with a n-member ensemble of short-range (background) forecasts $\mathbf{x}_i^b$, $i = 1, \ldots, n$, and an ensemble of predicted observations $\mathbf{y}_i^b = \mathbf{H}\mathbf{x}_i^b$ with the observation operator $\mathbf{H}$ transforming the model variables to observed quantities. The arguments that follow are restricted to the case that $\mathbf{H}$ is linear. (Nonlinear observation operators can also be handled if the EAKF is written in terms of an "extended" state, in which the observed variables are concatenated to the state vector.) Denote the ensemble mean by an overbar and deviations from that mean by a preceding δ; that is, $\mathbf{x}_i^b = \overline{\mathbf{x}}^b + \delta\mathbf{x}_i^b$ and $\mathbf{y}_i^b = \overline{\mathbf{y}}^b + \delta\mathbf{y}_i^b$. Given the observation vector $\mathbf{y}^o$, we update this ensemble to obtain an ensemble of analyses $\mathbf{x}_i^a$ whose mean and covariance are consistent with the Kalman filter.

The updated mean is

$$\overline{\mathbf{x}}^a = \overline{\mathbf{x}}^b + \mathbf{K}(\mathbf{y}^o - \overline{\mathbf{y}}^b), \tag{A1}$$

with the Kalman gain $\mathbf{K} = \mathbf{B}\mathbf{H}^{\mathrm{T}}(\mathbf{H}\mathbf{B}\mathbf{H}^{\mathrm{T}} + \mathbf{R})^{-1}$, where $\mathbf{B}$ and $\mathbf{R}$ are the background and observation error covariances, respectively. In the EnKF algorithms, $\mathbf{B}\mathbf{H}^{\mathrm{T}}$ is approximated by $1/(n-1)\sum_{i=1}^{n}\delta\mathbf{x}_i^b(\delta\mathbf{y}_i^b)^{\mathrm{T}}$, the sample covariance of $\mathbf{x}^b$ and $\mathbf{y}^b$, and similarly $\mathbf{H}\mathbf{B}\mathbf{H}^{\mathrm{T}}$ is approximated by $1/(n-1)\sum_{i=1}^{n}\delta\mathbf{y}_i^b(\delta\mathbf{y}_i^b)^{\mathrm{T}}$. The updated deviations are given by

$$\delta\mathbf{x}_i^a = \mathbf{F}\delta\mathbf{x}_i^b, \tag{A2}$$

where the adjustment matrix $\mathbf{F}$ is chosen so that the sample analysis covariance satisfies

$$\frac{1}{n-1}\sum_{i=1}^{n}\delta\mathbf{x}_i^a(\delta\mathbf{x}_i^a)^{\mathrm{T}} = \mathbf{A} = (\mathbf{I} - \mathbf{K}\mathbf{H})\mathbf{B}. \tag{A3}$$

The update Eqs. (A1) and (A2) each have the observation-space counterparts

$$\overline{\mathbf{y}}^a = \overline{\mathbf{y}}^b + \mathbf{H}\mathbf{K}(\mathbf{y}^o - \overline{\mathbf{y}}^b), \tag{A4}$$

and

$$\delta\mathbf{y}_i^a = \mathbf{F}_y\delta\mathbf{y}_i^b, \tag{A5}$$

where $\mathbf{F}_y$ is the observation-space adjustment matrix.

Combining Eqs. (A1) and (A2), the change in the model state vector for the ith member is given by

$$\mathbf{x}_i^a - \mathbf{x}_i^b = \mathbf{K}(\mathbf{y} - \overline{\mathbf{y}}^b) - (\mathbf{I} - \mathbf{F})\delta\mathbf{x}_i^b. \tag{A6}$$

Similarly, combining Eqs. (A4) and (A5), the change in the observed variables for the ith member is given by

$$\mathbf{y}_i^a - \mathbf{y}_i^b = \mathbf{HK}(\mathbf{y}^o - \overline{\mathbf{y}}^b) - (\mathbf{I} - \mathbf{F}_y)\delta\mathbf{y}_i^b. \quad (A7)$$

We restrict consideration to the case that $\delta\mathbf{x}_i^a = \delta\mathbf{x}_i^b$ when $\delta\mathbf{y}_i^b = \mathbf{H}\delta\mathbf{x}_i^b = 0$, so the analysis and forecast perturbations are equal when the forecast perturbation does not affect the observed quantities. In this case, the adjustment matrix $\mathbf{F}$ in Eq. (A2) can be written as

$$\mathbf{F} = \mathbf{I} - \tilde{\mathbf{K}}\mathbf{H}, \quad (A8)$$

for some $\tilde{\mathbf{K}}$ that will play the role of the gain in the update of the perturbations. Restricting to this case is crucial; otherwise, the update of perturbations in the null space of $\mathbf{H}$ is arbitrary and the relation between $\Delta\mathbf{x}_i = \mathbf{x}_i^a - \mathbf{x}_i^b$ and $\Delta\mathbf{y}_i = \mathbf{y}_i^a - \mathbf{y}_i^b$, which we seek to derive, will not hold.

Whitaker and Hamill (2002) quote the result of Andrews (1968) for an explicit form for $\tilde{\mathbf{K}}$:

$$\tilde{\mathbf{K}} = \mathbf{BH}^{\mathrm{T}}\mathbf{D}^{-1/2}(\mathbf{D}^{1/2} + \mathbf{R}^{1/2})^{-1}, \quad (A9)$$

where we have written $\mathbf{D} = \mathbf{HBH}^{\mathrm{T}} + \mathbf{R}$ for brevity. A similar expression holds in observation space for the adjustment matrix $\mathbf{F}_y = \mathbf{I} - \tilde{\mathbf{K}}_y$ with $\tilde{\mathbf{K}}_y = \mathbf{H}\tilde{\mathbf{K}}$.

Given the form for $\mathbf{F}$ and $\mathbf{F}_y$, Eqs. (A6) and (A7) can be rewritten as

$$\Delta\mathbf{x}_i \equiv \mathbf{x}_i^a - \mathbf{x}_i^b = \mathbf{K}(\mathbf{y} - \overline{\mathbf{y}}^b) - \tilde{\mathbf{K}}\mathbf{H}\delta\mathbf{x}_i^b, \quad (A10)$$

$$\Delta\mathbf{y}_i \equiv \mathbf{y}_i^a - \mathbf{y}_i^b = \mathbf{K}_y(\mathbf{y} - \overline{\mathbf{y}}^b) - \tilde{\mathbf{K}}_y\delta\mathbf{y}_i^b, \quad (A11)$$

where $\mathbf{K}_y = \mathbf{HK}$.

The remaining steps are simply algebra. Rearranging Eq. (A11) to solve for $\mathbf{y} - \overline{\mathbf{y}}^b$ and applying $\mathbf{K}$ to the result yields

$$\mathbf{K}(\mathbf{y} - \overline{\mathbf{y}}^b) = \mathbf{KK}_y^{-1}\Delta\mathbf{y}_i + \mathbf{KK}_y^{-1}\tilde{\mathbf{K}}_y\delta\mathbf{y}_i^b.$$

Substituting this result into the rhs of Eq. (A10) then gives

$$\Delta\mathbf{x}_i = \mathbf{KK}_y^{-1}\Delta\mathbf{y}_i + (\mathbf{KK}_y^{-1}\tilde{\mathbf{K}}_y - \tilde{\mathbf{K}})\delta\mathbf{y}_i^b. \quad (A12)$$

Now,

$$\mathbf{KK}_y^{-1} = \mathbf{BH}^{\mathrm{T}}\mathbf{D}^{-1}(\mathbf{BH}^{\mathrm{T}}\mathbf{D}^{-1})^{-1} = \mathbf{BH}^{\mathrm{T}}(\mathbf{HBH}^{\mathrm{T}})^{-1}$$

Thus,

$$\mathbf{KK}_y^{-1}\tilde{\mathbf{K}}_y = \mathbf{BH}^{\mathrm{T}}\mathbf{D}^{-1/2}(\mathbf{D}^{1/2} + \mathbf{R}^{1/2})^{-1} = \tilde{\mathbf{K}}$$

and Eq. (A12) becomes

$$\Delta\mathbf{x}_i = \mathbf{BH}^{\mathrm{T}}(\mathbf{HBH}^{\mathrm{T}})^{-1}\Delta\mathbf{y}_i. \quad (A13)$$

REFERENCES

Aberson, S. D., 2010: 10 years of hurricane synoptic surveillance (1997–2006). *Mon. Wea. Rev.,* **138,** 1536–1549.

Anderson, J. L., 2001: An ensemble adjustment Kalman filter for data assimilation. *Mon. Wea. Rev.,* **129,** 2884–2903.

——, 2003: A local least squares framework for ensemble filtering. *Mon. Wea. Rev.,* **131,** 634–642.

——, 2009: Spatially and temporally varying adaptive covariance inflation for ensemble filters. *Tellus,* **61A,** 72–83.

——, and N. Collins, 2007: Scalable implementations of ensemble filter algorithms for data assimilation. *J. Atmos. Oceanic Technol.,* **24,** 1452–1463.

——, T. Hoar, K. Raeder, H. Liu, N. Collins, R. Torn, and A. Arellano, 2009: The Data Assimilation Research Testbed: A community facility. *Bull. Amer. Meteor. Soc.,* **90,** 1283–1296.

Andrews, A., 1968: A square root formulation of the Kalman covariance equations. *AIAA J.,* **6,** 1165–1168.

Aravéquia, J. A., I. Szunyogh, E. J. Fertig, E. Kalnay, D. Kuhl, and E. J. Kostelich, 2011: Evaluation of a strategy for the assimilation of satellite radiance observations with the local ensemble transform Kalman filter. *Mon. Wea. Rev.,* **139,** 1932–1951.

Barker, D., and Coauthors, 2012: The Weather Research and Forecasting Model's Community Variational/Ensemble Data Assimilation System: WRFDA. *Bull. Amer. Meteor. Soc.,* **93,** 831–843.

Bennartz, R., 2000: Optimal convolution of AMSU-B to AMSU-A. *J. Atmos. Oceanic Technol.,* **17,** 1215–1225.

Berg, R., 2009: Tropical Cyclone Report Hurricane Ike (AL092008) 1–14 September 2008. NOAA/NHC, 55 pp. [Available online at http://www.nhc.noaa.gov/pdf/TCR-AL092008_Ike_3May10.pdf.]

Bishop, C. H., B. J. Etherton, and S. J. Majumdar, 2001: Adaptive sampling with the ensemble transform Kalman filter. Part I: Theoretical aspects. *Mon. Wea. Rev.,* **129,** 420–436.

Buehner, M., P. L. Houtekamer, C. Charette, H. L. Mitchell, and B. He, 2010a: Intercomparison of variational data assimilation and the ensemble Kalman filter for global deterministic NWP. Part I: Description and single-observation experiments. *Mon. Wea. Rev.,* **138,** 1550–1566.

——, ——, ——, ——, and ——, 2010b: Intercomparison of variational data assimilation and the ensemble Kalman filter for global deterministic NWP. Part II: One-month experiments with real observations. *Mon. Wea. Rev.,* **138,** 1567–1586.

Burgers, G., P. J. van Leeuwen, and G. Evensen, 1998: Analysis scheme in the ensemble Kalman filter. *Mon. Wea. Rev.,* **126,** 1719–1724.

Campbell, W. F., C. H. Bishop, and D. Hodyss, 2010: Vertical covariance localization for satellite radiances in ensemble Kalman filters. *Mon. Wea. Rev.,* **138,** 282–290.

Cavallo, S. M., J. Dudhia, and C. Snyder, 2011: A multilayer upper-boundary condition for longwave radiative flux to correct temperature biases in a mesoscale model. *Mon. Wea. Rev.,* **139,** 1952–1959.

——, R. D. Torn, C. Snyder, C. Davis, W. Wang, and J. Done, 2013: Evaluation of the Advanced Hurricane WRF data assimilation system for the 2009 Atlantic hurricane season. *Mon. Wea. Rev.,* in press.

Chen, F., and J. Dudhia, 2001: Coupling an advanced land-surface/hydrology model with the Penn State/NCAR MM5 modeling system. Part I: Model description and implementation. *Mon. Wea. Rev.,* **129,** 569–585.

Chen, Y., and C. Snyder, 2007: Assimilating vortex position with an ensemble Kalman filter. *Mon. Wea. Rev.,* **135,** 1828–1845.

Chou, M.-D., and M. J. Suarez, 1994: An efficient thermal infrared radiation parameterization for use in general circulation models. NASA Tech. Memo. 104606, Vol. 3, 85 pp.

Davis, C., W. Wang, J. Dudhia, and R. Torn, 2010: Does increased horizontal resolution improve hurricane wind forecasts? *Wea. Forecasting,* **25,** 1826–1841.

Dee, D. P., 2004: Variational bias correction of radiance data in the ECMWF system. *Proc. Workshop on Assimilation of High-Spectral-Resolution Sounders in NWP,* Reading, United Kingdom, ECMWF, 97–112.

——, and S. M. Uppala, 2009: Variational bias correction of satellite radiance data in the ERA-Interim reanalysis. *Quart. J. Roy. Meteor. Soc.,* **135,** 1830–1841.

——, and Coauthors, 2011: The ERA-Interim reanalysis: Configuration and performance of the data assimilation system. *Quart. J. Roy. Meteor. Soc.,* **137,** 553–597.

Derber, J. C., and W.-S. Wu, 1998: The use of TOVS cloud-cleared radiances in the NCEP SSI analysis system. *Mon. Wea. Rev.,* **126,** 2287–2299.

Evensen, G., 1994: Sequential data assimilation with a nonlinear quasi-geostrophic model using Monte Carlo methods to forecast error statistics. *J. Geophys. Res.,* **99** (C5), 10 143–10 162.

Eyre, J. R., 1992: A bias correction scheme for simulated TOVS brightness temperatures. Tech. Memo. 186, ECMWF, Reading, United Kingdom, 34 pp.

Fertig, E. J., B. R. Hunt, E. Ott, and I. Szunyogh, 2007: Assimilating non-local observations with a local ensemble Kalman filter. *Tellus,* **59A,** 719–730.

——, and Coauthors, 2009: Observation bias correction with an ensemble Kalman filter. *Tellus,* **61A,** 210–226.

Fiorino, M., 2009: Record-setting performance of the ECMWF IFS in medium-range tropical cyclone track prediction. *ECMWF Newsletter,* No. 118, ECMWF, Reading, United Kingdom, 20–27.

Gaspari, G., and S. E. Cohn, 1999: Construction of correlation functions in two and three dimensions. *Quart. J. Roy. Meteor. Soc.,* **125,** 723–757.

Goodrum, G., K. B. Kidwell, and W. Winston, Eds., 1999: *NOAA KLM User's Guide.* National Oceanic and Atmospheric Administration, CD-ROM.

Hamill, T. M., 1999: Hypothesis tests for evaluating numerical precipitation forecasts. *Wea. Forecasting,* **14,** 155–167.

——, J. S. Whitaker, M. Fiorino, and S. G. Benjamin, 2011a: Global ensemble predictions of 2009's tropical cyclones initialized with an ensemble Kalman filter. *Mon. Wea. Rev.,* **139,** 668–688.

——, ——, D. T. Kleist, M. Fiorino, and S. G. Benjamin, 2011b: Predictions of 2010's tropical cyclones using the GFS and ensemble-based data assimilation methods. *Mon. Wea. Rev.,* **139,** 3243–3247.

Han, Y., P. van Delst, Q. Liu, F. Weng, B. Yan, R. Treadon, and J. Derber, 2006: JCSDA Community Radiative Transfer Model (CRTM)—Version 1. NOAA Tech. Rep. NESDIS 122, 33 pp.

Harris, B. A., and G. Kelly, 2001: A satellite radiance-bias correction scheme for data assimilation. *Quart. J. Roy. Meteor. Soc.,* **127,** 1453–1468.

Hartung, D. C., J. A. Otkin, R. A. Petersen, D. D. Turner, and W. F. Feltz, 2011: Assimilation of surface-based boundary layer profiler observations during a cool-season weather event using an observing system simulation experiment. Part II: Forecast assessment. *Mon. Wea. Rev.,* **139,** 2327–2346.

Hong, S.-Y., J. Dudhia, and S.-H. Chen, 2004: A revised approach to ice microphysical processes for the bulk parameterization of clouds and precipitation. *Mon. Wea. Rev.,* **132,** 103–120.

——, Y. Noh, and J. Dudhia, 2006: A new vertical diffusion package with an explicit treatment of entrainment processes. *Mon. Wea. Rev.,* **134,** 2318–2341.

Houtekamer, P. L., and H. L. Mitchell, 1998: Data assimilation using an ensemble Kalman filter technique. *Mon. Wea. Rev.,* **126,** 796–811.

——, ——, G. Pellerin, M. Buehner, M. Charron, L. Spacek, and B. Hansen, 2005: Atmospheric data assimilation with an ensemble Kalman filter: Results with real observations. *Mon. Wea. Rev.,* **133,** 604–620.

Hunt, B. R., E. J. Kostelich, and I. Szunyogh, 2007: Efficient data assimilation for spatiotemporal chaos: A local ensemble transform Kalman filter. *Physica D,* **230,** 112–126.

Kain, J. S., and J. M. Fritsch, 1990: A one-dimensional entraining/detraining plume model and its application in convective parameterization. *J. Atmos. Sci.,* **47,** 2784–2802.

Li, J., and H. Liu, 2009: Improved hurricane track and intensity forecast using single field-of-view advanced IR sounding measurements. *Geophys. Res. Lett.,* **36,** L11813, doi:10.1029/2009GL038285.

Liou, K., 2002: *An Introduction to Atmospheric Radiation.* 2nd ed. Academic Press, 583 pp.

Liu, H., and J. Li, 2010: An improvement in forecasting rapid intensification of Typhoon Sinlaku (2008) using clear-sky full spatial resolution advanced IR soundings. *J. Appl. Meteor. Climatol.,* **49,** 821–827.

——, J. Anderson, Y.-H. Kuo, and K. Raeder, 2007: Importance of forecast error multivariate correlations in idealized assimilation of GPS radio occultation data with the ensemble adjustment filter. *Mon. Wea. Rev.,* **135,** 173–185.

Liu, Q., and F. Weng, 2006: Advanced doubling-adding method for radiative transfer in planetary atmosphere. *J. Atmos. Sci.,* **63,** 3459–3465.

Liu, Z., and F. Rabier, 2002: The interaction between model resolution, observation resolution and observation density in data assimilation: A one-dimensional study. *Quart. J. Roy. Meteor. Soc.,* **128,** 1367–1386.

——, H.-C. Lin, Y.-H. Kuo, D. H. Bromwich, and L. Bai, 2011: Data assimilation over northern polar region using WRF and WRFDA. *Extended Abstracts, 12th WRF Users' Workshop,* Boulder, CO, National Center for Atmospheric Research, 1–8.

Lorenc, A. C., 2003: The potential of the ensemble Kalman filter for NWP—A comparison with 4D-VAR. *Quart. J. Roy. Meteor. Soc.,* **129,** 3183–3203.

McNally, A. P., J. C. Derber, W. Wu, and B. B. Katz, 2000: The use of TOVS level-1b radiances in the NCEP SSI analysis system. *Quart. J. Roy. Meteor. Soc.,* **126,** 689–724, doi:10.1002/qj.49712656315.

McNally, T., 2007: The use of satellite data in polar regions. *Proc. ECMWF Seminar on Polar Meteorology,* Reading, United Kingdom, ECMWF, 103–114.

Miyoshi, T., and Y. Sato, 2007: Assimilating satellite radiances with a Local Ensemble Transform Kalman Filter (LETKF) applied to the JMA Global Model (GSM). *SOLA,* **3,** 37–40.

——, ——, and T. Kadowaki, 2010: Ensemble Kalman filter and 4D-Var intercomparison with the Japanese Operational Global Analysis and Prediction System. *Mon. Wea. Rev.,* **138,** 2846–2866.

Mlawer, E. J., S. J. Taubman, P. D. Brown, M. J. Iacono, and S. A. Clough, 1997: Radiative transfer for inhomogeneous atmosphere: RRTM, a validated correlated-*k* model for the longwave. *J. Geophys. Res.,* **102** (D14), 16 663–16 682.

Otkin, J. A., 2010: Clear and cloudy sky infrared brightness temperature assimilation using an ensemble Kalman filter. *J. Geophys. Res.,* **115,** D19207, doi:10.1029/2009JD013759.

——, 2012: Assessing the impact of the covariance localization radius when assimilating infrared brightness temperature observations using an ensemble Kalman filter. *Mon. Wea. Rev.,* **140,** 543–561.

Parrish, D. F., and S. E. Cohn, 1985: A Kalman filter for a two-dimensional shallow-water model: Formulation and preliminary experiments. Office Note 304, Washington, DC, National Meteorological Center, 64 pp.

——, and J. C. Derber, 1992: The National Meteorological Center's spectral statistical interpolation analysis system. *Mon. Wea. Rev.,* **120,** 1747–1763.

Poli, P., S. B. Healy, and D. P. Dee, 2010: Assimilation of Global Positioning System radio occultation data in the ECMWF ERA-Interim reanalysis. *Quart. J. Roy. Meteor. Soc.,* **136,** 1972–1990.

Puri, K., J. Barkmeijer, and T. N. Palmer, 2001: Ensemble prediction of tropical cyclones using targeted diabatic singular vectors. *Quart. J. Roy. Meteor. Soc.,* **127,** 709–731.

Rappaport, E. N., and Coauthors, 2009: Advances and challenges at the National Hurricane Center. *Wea. Forecasting,* **24,** 395–419.

Schwartz, C. S., Z. Liu, Y. Chen, and X.-Y. Huang, 2012: Impact of assimilating microwave radiances with a limited-area ensemble data assimilation system on forecasts of Typhoon Morakot. *Wea. Forecasting,* **27,** 424–437.

Skamarock, W. C., and Coauthors, 2008: A description of the Advanced Research WRF version 3. NCAR Tech. Note NCAR/TN-475+STR, 113 pp. [Available from UCAR Communications, P. O. Box 3000, Boulder, CO 80307.]

Smith, W. L., H. M. Woolf, C. M. Hayden, D. Q. Wark, and L. M. McMillin, 1979: The TIROS-N operational vertical sounder. *Bull. Amer. Meteor. Soc.,* **60,** 1177–1187.

Tippett, M. K., J. L. Anderson, C. H. Bishop, T. M. Hamill, and J. S. Whitaker, 2003: Ensemble square root filters. *Mon. Wea. Rev.,* **131,** 1485–1490.

Torn, R. D., 2010: Performance of a mesoscale ensemble Kalman filter (EnKF) during the NOAA High-Resolution Hurricane Test. *Mon. Wea. Rev.,* **138,** 4375–4392.

——, and G. J. Hakim, 2008: Performance characteristics of a pseudo-operational ensemble Kalman filter. *Mon. Wea. Rev.,* **136,** 3947–3963.

——, and ——, 2009: Ensemble data assimilation applied to RAINEX observations of Hurricane Katrina (2005). *Mon. Wea. Rev.,* **137,** 2817–2829.

——, ——, and C. Snyder, 2006: Boundary conditions for limited-area ensemble Kalman filters. *Mon. Wea. Rev.,* **134,** 2490–2502.

Van der Grijn, G., J. E. Paulsen, F. Lalaurette, and M. Leutbecher, 2005: Early medium-range forecasts of tropical cyclones. *ECMWF Newsletter,* No. 102, ECMWF, Reading, United Kingdom, 7–14.

Wang, X., 2011: Application of the WRF Hybrid ETKF–3DVAR data assimilation system for hurricane track forecasts. *Wea. Forecasting,* **26,** 868–884.

——, D. M. Barker, C. Snyder, and T. M. Hamill, 2008: A hybrid ETKF–3DVAR data assimilation scheme for the WRF model. Part I: Observing system simulation experiment. *Mon. Wea. Rev.,* **136,** 5116–5131.

Whitaker, J. S., and T. M. Hamill, 2002: Ensemble data assimilation without perturbed observations. *Mon. Wea. Rev.,* **130,** 1913–1924.

Zapotocny, T. H., J. A. Jung, J. F. Le Marshall, and R. E. Treadon, 2008: A two-season impact study of four satellite data types and rawinsonde data in the NCEP Global Data Assimilation System. *Wea. Forecasting,* **23,** 80–100.

Zhang, F., Y. Weng, J. A. Sippel, Z. Meng, and C. H. Bishop, 2009: Cloud-resolving hurricane initialization and prediction through assimilation of Doppler radar observations with an ensemble Kalman filter. *Mon. Wea. Rev.,* **137,** 2105–2125.

——, ——, Y.-H. Kuo, J. S. Whitaker, and B. Xie, 2010: Predicting Typhoon Morakot's catastrophic rainfall with a convection-permitting mesoscale ensemble system. *Wea. Forecasting,* **25,** 1816–1825.

——, ——, J. F. Gamache, and F. D. Marks, 2011: Performance of convection-permitting hurricane initialization and prediction during 2008–2010 with ensemble data assimilation of inner-core airborne Doppler radar observations. *Geophys. Res. Lett.,* **38,** L15810, doi:10.1029/2011GL048469.

Zupanski, D., M. Zupanski, L. D. Grasso, R. Brummer, I. Jankov, D. Lindsey, M. Sengupta, and M. Demaria, 2011: Assimilating synthetic GOES-R radiances in cloudy conditions using an ensemble-based method. *Int. J. Remote Sens.,* **32** (24), 9637–9659.